

THE OFFICIAL MAGAZINE OF THE OCEANOGRAPHY SOCIETY

Oceanography

CITATION

Münchow, A., L. Padman, P. Washam, and K.W. Nicholls. 2016. The ice shelf of Petermann Gletscher, North Greenland, and its connection to the Arctic and Atlantic Oceans. *Oceanography* 29(4):84–95, <https://doi.org/10.5670/oceanog.2016.101>.

DOI

<https://doi.org/10.5670/oceanog.2016.101>

COPYRIGHT

This article has been published in *Oceanography*, Volume 29, Number 4, a quarterly journal of The Oceanography Society. Copyright 2016 by The Oceanography Society. All rights reserved.

USAGE

Permission is granted to copy this article for use in teaching and research. Republication, systematic reproduction, or collective redistribution of any portion of this article by photocopy machine, reposting, or other means is permitted only with the approval of The Oceanography Society. Send all correspondence to: info@tos.org or The Oceanography Society, PO Box 1931, Rockville, MD 20849-1931, USA.

THE ICE SHELF OF PETERMANN GLETSCHER, NORTH GREENLAND, AND ITS CONNECTION TO THE ARCTIC AND ATLANTIC OCEANS

By Andreas Münchow, Laurie Padman, Peter Washam, and Keith W. Nicholls

Petermann Gletscher, August 10,
2015. View is to the northeast
from the center of the glacier.

“...the new remotely sensed and in situ data identify the Petermann ice-ocean system as a dynamically rich and rapidly changing environment.”

ABSTRACT. Petermann Gletscher in North Greenland features the second largest floating ice shelf in the Northern Hemisphere. This paper describes the history of its exploration and presents new ocean and glacier observations. We find that the floating ice shelf is strongly coupled to the ocean below and to Nares Strait at time scales from tidal to interannual. Our observations cover the 2012 to 2016 period after two large calving events took place in 2010 and 2012 that reduced the ice shelf area by 380 km² to about 870 km² today. A potential third breakup, of an additional 150 km², is anticipated by a large fracture that extends from the margin to the center of the glacier.

HISTORY OF EXPLORATION

In 1921 owing to starvation I had to go directly from Cape Heiberg-Juergensen to our cache at Cape Agassiz...during this journey the greater part of the glacier was mapped. – Lauge Koch

Traveling by dog sled, Danish geologist Lauge Koch mapped Petermann Gletscher in 1921 as he crossed it with three Inuit companions on a journey to explore northern North Greenland. They discovered and named Steensby, Ryder, and H.C. Ostenfeld Glaciers (Figure 1) that, like Petermann Gletscher, had floating ice shelves (Ahnert, 1963; Higgins, 1990). All four starved travelers returned home safely in 1921; however, their previous expedition in 1917 had not been so lucky, because two traveling companions died (Rasmussen, 1921). Figure 2 shows the 1917 and 1921 survey tracks along with the historic Koch (1928) map and a modern remotely sensed mapping of Petermann Gletscher and its fjord.

Only 30 years after these dog-sled

expeditions, the onset of the Cold War brought airplanes and radar to North Greenland. Even further north, the Arctic Ocean along with the bordering land and ice masses of Greenland and Canada became a battle space. To support military aviation, weather stations were established in 1947 at Eureka and in 1950 at Alert (J. Johnson, 1990). In 1951, more than 12,000 US military men and women descended on the small trading post of Thule (Figure 1) that Knud Rasmussen and Peter Freuchen had established 40 years earlier to support their dog-sled expeditions across Greenland (Freuchen, 1935). “Operation Blue Jay” built Thule Air Force Base (AFB) as a forward station for fighter jets, nuclear-armed bombers, and early warning radar systems. The radars were designed to detect ballistic missiles crossing the Arctic Ocean from Eurasia to North America, while the bombers were to retaliate in case of a nuclear attack from the Soviet Union.

Today, the jets, bombers, and Soviet Union are all gone, but Thule AFB is still

there as the gateway to North Greenland. It is also the only deepwater port within a 1,600 km radius, allowing US, Canadian, Danish, and Swedish ships to receive and discharge their sailors and scientists. Since 2009, Thule AFB has also served as the northern base for annual Operation IceBridge flights over North Greenland that map the changing ice sheets and glaciers.

The establishment of military weather stations and airfields in the high Arctic coincided with the discovery of massive ice islands (large tabular icebergs) drifting freely in the Arctic Ocean. On August 14, 1946, airmen of the 46th Strategic Reconnaissance Squadron of the US Air Force discovered a moving ice island with an area of about 200 km² that was kept secret until November 1950 (Hattersley-Smith et al., 1952). Most ice islands originated from ice shelves to the north of Ellesmere Island whose area was reduced over the last century from about 8,900 km² to 1,000 km² (Jeffries, 1992; Antoniadis et al., 2011). Franz Boas provided the first historical description of an ice island from Petermann Gletscher in 1883 when he established a German station in Cumberland Sound at 65°N, 65°W as part of the First International Polar Year (Boas, 1885). Without knowing the source of the massive tabular iceberg, Boas (1885) made measurements of ice thickness (120–150 m), extent

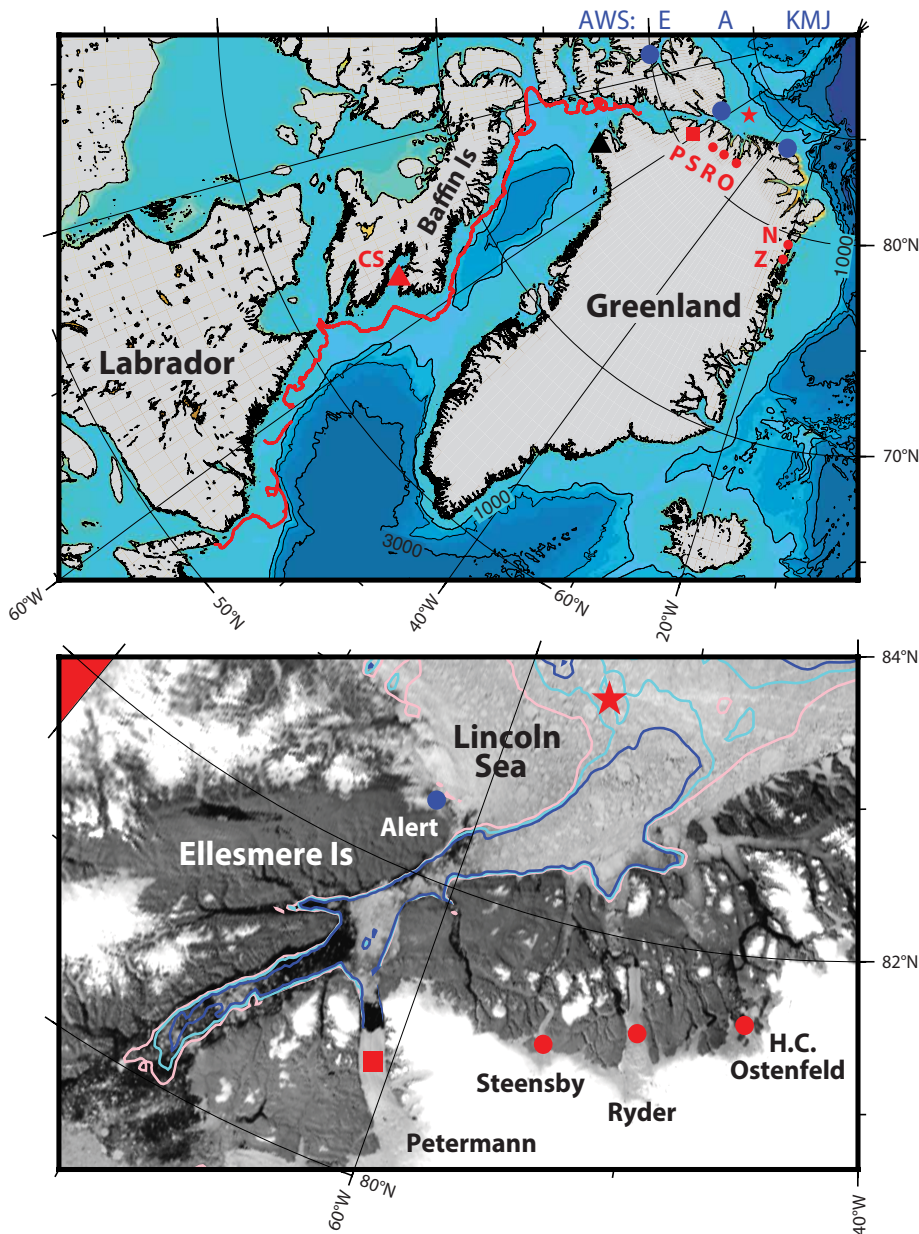


FIGURE 1. (top) Map of the study area from the Arctic to the Atlantic Ocean with bathymetry contoured in 1,000 m intervals. The red square indicates Petermann Gletscher, and red tracks show the 2010/11 path of Petermann Ice Island PII-2010A. Blue dots show locations of weather stations (west to east near 80°N) at Eureka (E), Alert (A), and Kap Morris Jesup (KMJ). Thule Air Force Base is located near 76°N and shown as a black triangle. Red dots indicate glaciers with current floating ice shelves or that have had floating ice shelves within the last 20 years, includes Petermann (P), Steensby (S), Ryder (R), and H.C. Ostenfeld (O), 79 North Glacier (N), and Zachariae Isstrom (Z). The red triangle in Cumberland Sound (CS) shows the location of the ice island described by Boas (1885). The bottom panel shows details west of 40°W. The northern sill in the Lincoln Sea is indicated by a red star. Bathymetry contours of 250 m (rose), 300 m (cyan), and 350 m (blue) are plotted over a MODIS image from August 2015.

(78 km²), surface undulations (150 m wavelength over several kilometers), and rocks both on the ice surface and within the upper 1–2 m of the ice. All these features match scales and characteristics of the Petermann Gletscher ice shelf as they were first described by Richard Croppinger, surgeon of a British Naval

expedition in 1874/75. Croppinger identified the terminus of Petermann Gletscher as a floating ice shelf when he noticed vertical tidal motions of the glacier from sextant measurements (Nares, 1876).

Here, we extend these initial explorations with modern observations of the shape of the ice shelf as well as the ocean

below it. These new observations are neither complete nor fully understood in their dynamical implications; however, the new remotely sensed and in situ data identify the Petermann ice-ocean system as a dynamically rich and rapidly changing environment. These tantalizing observations suggest strong ocean impacts on the ice shelf as the coupled system responds to larger-scale change observed over Greenland (Hanna et al., 2013) and the Arctic Ocean (Polyakov et al., 2010).

PETERMANN ICE SHELF

Historically, the floating section of Petermann Gletscher oscillated in length between 70 km and 85 km from the grounding line at decadal time scales (Münchow et al., 2014) as the glacier's terminus moved steadily seaward at speeds of 900–1,000 m yr⁻¹ (Higgins, 1990). This changed when two large calving events reduced the length of the ice shelf in 2010 and 2012 from 81 km to 46 km (Münchow et al., 2014). The ice lost from 2010 to 2012, 36 ± 4 Gt, represents three years of ice flux across the grounding line (Rignot and Steffen, 2008); however, it will take the glacier roughly two decades to reach its former terminus location, if it continues to advance at its current speed of ~1.2 km yr⁻¹ (Nick et al., 2012).

The structure and extent of the ice shelf depend on the interactions of numerous processes, including atmospheric and oceanic forcing, sea ice and mélange (the combination of sea ice and small iceberg fragments) in the fjord, and the dynamics of ice sheet flow across the grounding line (Straneo et al., 2013). Here, we provide new observations on the most difficult of these processes to observe, the interactions between the ocean and the ice shelf. H. Johnson et al. (2011) and Münchow (2016) discuss the regional oceanography of Petermann Fjord and Nares Strait, respectively, with data collected prior to the 2010 calving event. Our new observations were obtained since the 2012 calving event, and extend throughout Petermann Fjord and under the ice shelf.

Petermann Fjord connects the glacier to Nares Strait, which in turn is connected to the Arctic Ocean in the north and the Atlantic Ocean via Baffin Bay in the south (Figure 1). The path of Petermann Ice Island PII-2010A emphasizes this connection, as the 60 m thick section of the ice island reached the Labrador Sea in the south within nine months of its calving in 2010. PII-2010 left Petermann Fjord on September 9, 2010, breaking into segments A and B while pivoting around Joe Island (Crawford et al., 2016). It flushed out of Nares Strait 10 days later; at this time, an ARGOS-tracked transponder was placed on it to monitor its changing position. PII-2010A moved southward with the Baffin Island Current (Münchow et al., 2015) at an average speed of $\sim 0.11 \text{ m s}^{-1}$ and passed Davis Strait. Remaining on the continental shelf of the Labrador Sea, it passed Cumberland Sound, Labrador, where Boas (1885) reported the first observed Petermann Gletscher ice island (Figure 1). It reached Newfoundland in August of 2011 before finally melting away in a coastal cove about 3,000 km from its Petermann Fjord birthplace. PII-2010B followed a similar track, albeit at much slower speeds as it became grounded off Baffin Island in water 91 m deep (Crawford et al., 2016).

Petermann Gletscher drains about 4% of the Greenland ice sheet via a network of glacial channels and streams that extend some 750 km landward from the grounding line (Bamber et al., 2013). The glacier goes afloat at the grounding zone (Figure 2) where bedrock, till, and ice meet the ocean waters $\sim 600 \text{ m}$ below sea level (Rignot, 1996). Rignot and Steffen (2008) describe the floating section of Petermann Gletscher, which contains several major surface and subglacial channels running from near the grounding zone to the terminus. In numerical models these 1–3 km wide channels are regions of enhanced basal melting (Gladish et al., 2012; Millgate et al., 2013); however, laser altimeter observations from repeat tracks both along a central channel and along the ambient ice shelf

reveal identical glacier thinning between 2007 and 2010 (Münchow et al., 2014), prior to the large calving events. More recently, as part of NASA's Operation IceBridge, a laser altimeter was used to measure surface elevation from the grounded ice to the ice front on a repeat path along the glacier in April 2013 and May 2014 (Figure 3). Assuming the ice to be freely floating, we estimate ice basal topography and find that ice draft varies from 200 m at the modern terminus to 600 m at the grounding zone near distance zero (Figure 3). The 2013 profile was shifted seaward by 1.25 km to match the 2014 terminus position. The annual averaged terminus speed is thus $1.25 \pm 0.02 \text{ km}$ over 387 days or $1,180 \pm 20 \text{ m yr}^{-1}$. Note the close correspondence of large and small crevasses in 2013 and 2014 near 18, 22, 28, and 40 km from the grounding zone, which suggests that the

2013/14 terminus speed also represents glacier speeds at those locations.

Between August 20, 2015, and February 11, 2016, we measured glacier speeds 16 km from the grounding zone with a single-frequency GPS as part of an ocean weather observatory (discussed below). The displacement during these 175 days was $564 \pm 5 \text{ m}$, which corresponds to a speed of $1,178 \pm 10 \text{ m yr}^{-1}$. From 102 days of data collected between November 2015 and February 2016, we estimate the winter-only displacement of $330 \pm 5 \text{ m}$, which corresponds to $1,180 \pm 18 \text{ m yr}^{-1}$. This 2015/16 estimate 16 km from the grounding line is identical to the 2013/14 estimate of the terminus within the uncertainty. Our final glacier speed estimate originates from three dual-frequency geodetic GPS receivers that provide centimeter accuracy at 30-second intervals; however, we only have time

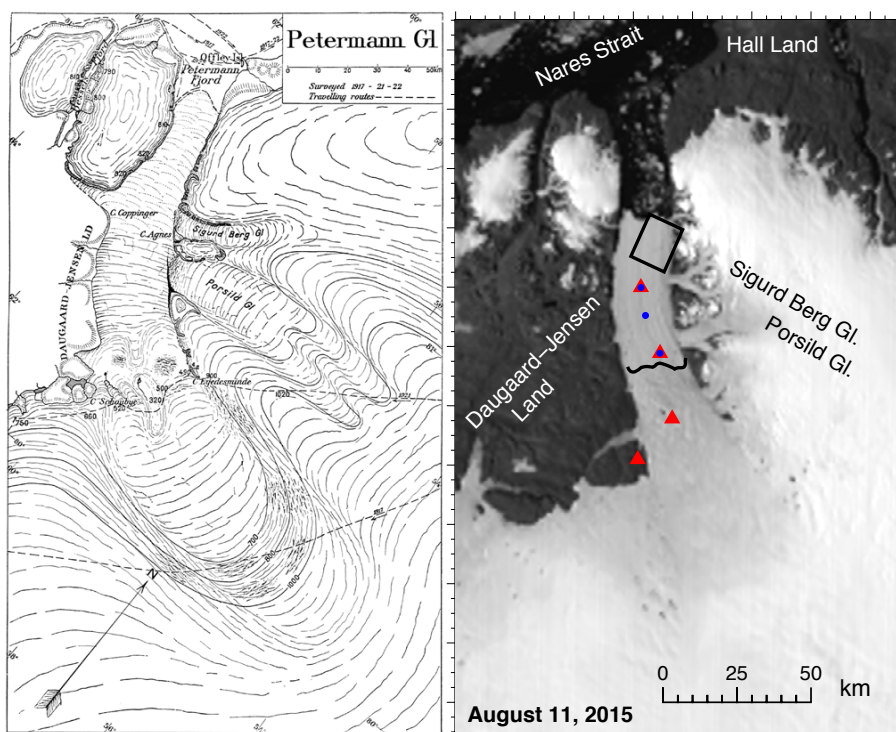


FIGURE 2. (left) Petermann Gletscher as mapped by Lauge Koch from dog-sled excursions in 1917 and 1921 (Koch, 1928), with tracks marked as faint dashed lines. (right) Satellite (MODIS-Terra) imagery of Petermann Gletscher for August 11, 2015. The scale for both maps is 1:1,250,000. The right panel shows the locations of three GPS stations (red triangles) and three Ocean Weather Stations (blue dots) deployed on the glacier in 2015 as well as a bedrock reference GPS station on Dagaard-Jensen Land at Kap Schoubye (also a red triangle). The GPS stations measured vertical and horizontal glacier motion while the Ocean Weather Stations measure ocean properties below the floating glacier via sensors cabled to surface data loggers. The solid black line in the right panel shows the location of the grounding zone, and the black box outlines the location of the Landsat image shown in Figure 8.

series for the 13 days that the instruments were deployed in August 2015 (see Figure 2 for locations). These data were processed using GAMIT/TRACK software following methodology outlined by King (2004). For the 13 days of measurements, we find the glacier moving 26 m at a site landward of the grounding line, 44 m at the grounding line, and 43 m at the site seaward of the grounding line. The uncertainty for each displacement is 0.0026 m, which we estimate from bedrock reference station data. Our short summer snapshots of glacier motion then represent speeds of 732, 1,235, and $1,208 \pm 1 \text{ m yr}^{-1}$, with the speed

maximum at the grounding line.

In Figure 3 we compare these 2013/14 and 2015/16 ice velocities with 2000 to 2008 estimates obtained from RADARSAT interferometry using winter image pairs generally separated by ~ 90 days between December and April (Joughin et al., 2010). We extract the RADARSAT glacier speed estimates along a flow line that contains our dual- and single-frequency GPS receivers. Uncertainty of the RADARSAT speed estimates are 3% of flow speeds (Joughin et al., 2010) or 20 m yr^{-1} to 35 m yr^{-1} for Petermann Gletscher. Speeds prior to 2010 were stable at about $1,050 \pm 32 \text{ m yr}^{-1}$, about $12 \pm 5\%$ less than

the $1,180 \pm 20 \text{ m yr}^{-1}$ we observe after the 2010 and 2012 calving events from airborne laser altimeter and winter-only GPS (Figure 3).

Our 13-day summer velocity estimates for August 2015 from the three geodetic GPS receivers reveal an along-glacier velocity profile across the grounding line that is consistent with the shape from the 2000 to 2008 RADARSAT velocity profiles along the same flow line; however, our summer speeds are larger than the winter RADARSAT speeds. Ahlström et al. (2013) observed similar seasonal variations from a year-long GPS 2011/12 record recovered from the ice shelf of Petermann Gletscher. The acceleration of the glacier from June to August is assumed to occur when surface meltwater percolates to the bedrock, increases lubrication, and thus reduces friction (Nick et al., 2012).

Vertical glacier and ice shelf displacement was also recorded, with accuracy of 2–3 cm, by the three 13-day geodetic GPS records from August 2015 (Figure 4). The observed full range of vertical glacier displacements diminishes from almost 2 m about 26 km seaward of the grounding zone (GZ+26) to 0.6 m in the grounding zone (GZ-00) to nil (within the uncertainty) at GZ-20, about 20 km landward of the grounding zone. The reduced vertical and increased horizontal (not shown) tidal oscillations at GZ-00 reflect active flexing of the glacier (Fricker and Padman, 2006).

The ice shelf motion at GZ+26 is dominated by the principal lunar semidiurnal M_2 tide, which has a period of 12.42 hours. The modulation of tide height maxima and minima is the spring-neap cycle caused by superposition of the principal solar semidiurnal tide, S_2 , which has a period of 12.00 hours. There is, also, a noticeable diurnal inequality in high tides, indicating the presence of diurnal tides K_1 and O_1 , with periods of about 23.93 hours and 25.82 hours, respectively. Future studies will examine harmonic constituents, but preliminary results reveal that the amplitudes and phases of the tidal signals at GZ+26 are close to

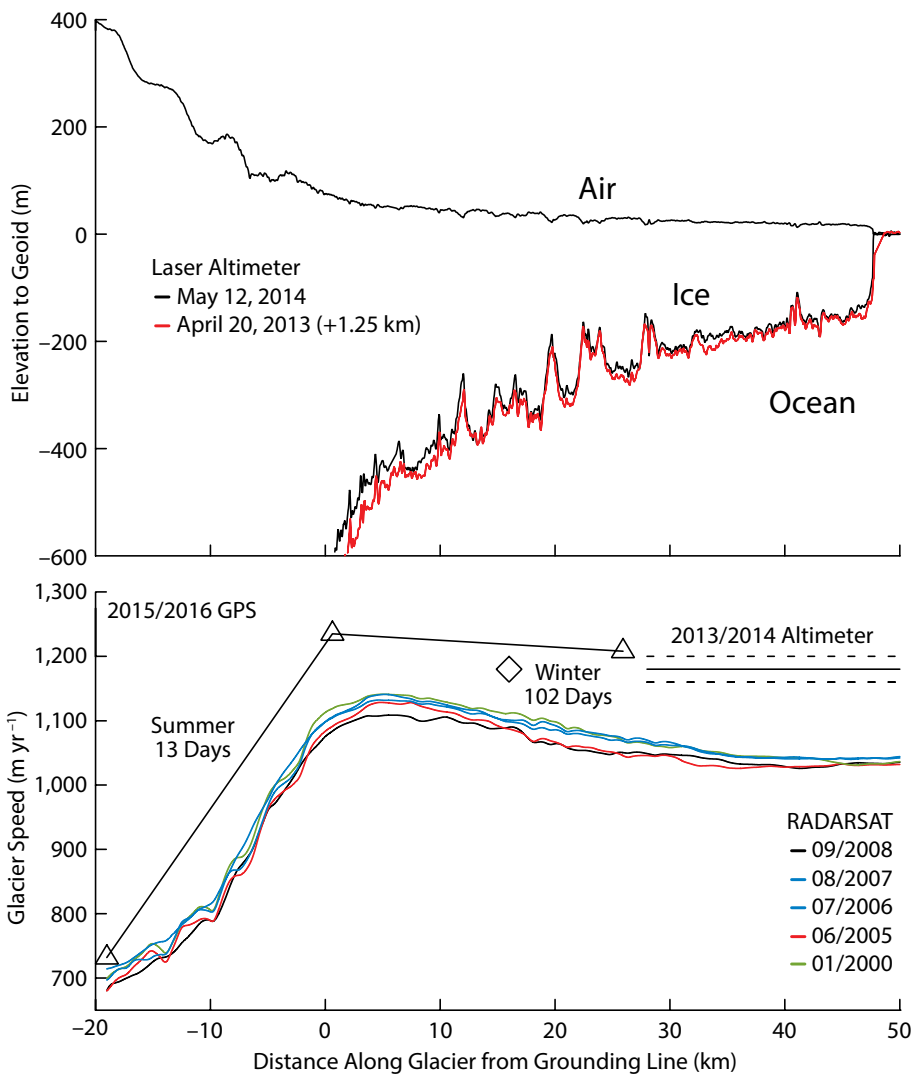


FIGURE 3. Surface and basal elevation profile (top) and speed (bottom) of Petermann Gletscher along its axis. Distances are in kilometers relative to the grounding zone. In the lower panel, speeds from three dual-frequency GPS stations deployed for 13 days in summer of 2015 are shown as triangles while speed from a single-frequency GPS averaged for 102 days in the winter of 2015/16 is shown as a diamond. GPS locations are shown in Figure 2. A speed estimate from two repeat laser altimeters is shown as a solid black line with dashed lines indicating a 20 m yr^{-1} uncertainty.

those observed at Discovery Harbor off Ellesmere Island at 81.7°N latitude in the nineteenth (Greely, 1888), twentieth (Harris, 1911), and twenty-first centuries. More specifically, the dominant semi-diurnal M_2 tide at GZ+26 and Discovery Harbor have amplitudes of 0.615 m and 0.609 m, while their Greenwich phases are 113° and 106°. The 7° phase difference expresses a time difference of less than 15 minutes that can be explained by the tidal wave propagating from Nares Strait into Petermann Fjord and into the cavity of the glacier. We conclude that the ice shelf at GZ+26 oscillates freely with the ambient ocean tide in Petermann Fjord without frictional impedence.

In summary, historical and modern observations reveal substantial change in the extent of Petermann's floating ice shelf and ice-shelf motions at tidal to inter-annual time scales. Future studies will more comprehensively quantify both the time rate of change of glacier motions and its forcing via formal time series analyses.

OCEAN OBSERVATIONS IN NARES STRAIT AND PETERMANN FJORD

Warm Atlantic waters enter the Arctic Ocean to the west of Norway and Svalbard (Straneo and Heimbach, 2013) and turn eastward, and a core of maximum subsurface temperature marks their circulation counterclockwise along topographic slopes (Coachman and Barnes, 1963; Polyakov et al., 2010). At the end of this pathway lies the Lincoln Sea and the northern entrance of Nares Strait. Atlantic waters can enter Nares Strait only after passing over a 290 m deep sill (Figure 1). This sill in the Lincoln Sea is the deepest connection of Petermann Fjord with the Atlantic Ocean, because a 220 m deep sill in southern Nares Strait prevents Atlantic waters from entering via Baffin Bay in the south (Münchow et al., 2011).

Flow of Atlantic waters into Nares Strait and into Petermann Fjord thus originates from the Lincoln Sea in the north where deep ocean temperatures at sill depth frequently exceed 0.3°C

(de Steur et al., 2013). This water is warm relative to the -2.2°C pressure-dependent in situ freezing point at the base of the ice shelf. Estimates of heat flux into the fjord vary from $3 \pm 0.5 \times 10^{11} \text{ J s}^{-1}$ (H. Johnson et al., 2011) to $6 \pm 0.5 \times 10^{11} \text{ J s}^{-1}$. This observed heat flux is three times larger than the $1.1 \times 10^{11} \text{ J s}^{-1}$ required to melt the $\sim 12 \text{ Gt yr}^{-1}$ of ice that crosses the grounding line: for the ice shelf at its historical minimum extent of $\sim 70 \text{ km}$ long and 15 km wide, this is equivalent to an aerial average melt rate of 9.7 m yr^{-1} . This is about 5% larger than the steady-state value of 9.2 m yr^{-1} that Rignot et al. (2001) calculated from satellite-derived ice thickness and velocity, but less than the 13 m yr^{-1} that Münchow et al. (2014) obtained using steady-state flux gate calculations and non-steady satellite altimeter measurements along repeat tracks. The presently unused portion of the heat flux into the fjord suggests the potential for greater losses from the ice shelf, particularly if ocean circulation and/or stratification change to accelerate the interaction between the ocean water and the ice shelf. Shroyer et al. (in press) suggest that shifts in the sea-ice cover in Nares

Strait may induce such change.

The warm Atlantic sourced waters in Nares Strait enter Petermann Fjord across a 440 m deep sill that was mapped in August 2015 at 10 m horizontal resolution with a Kongsberg EM 122 multi-beam sonar system mounted to the hull of the Swedish icebreaker *Oden*. Sections of potential density, salinity, and temperature along the center of the fjord, across the sill, and into Nares Strait were obtained in August 2012. These data emphasize the dominant presence of warm and salty waters of Atlantic origin inside the fjord (Figure 5). Nares Strait ocean bottom temperatures reach $+0.26^{\circ}\text{C}$ with salinities up to 34.76 psu, but there was no evidence of these waters entering Petermann Fjord at that time. Instead, the deep water crossing the sill to fill the fjord in 2012 had salinities reaching 34.72 psu and temperatures near $+0.20^{\circ}\text{C}$ extending to the front of the ice shelf. The lack of observations within about 10 km of the sill in 2012 was a result of a 150 km^2 ice island with a 200 m draft occupying much of the fjord (Münchow et al., 2014). Nevertheless, at 350 m depth there was a lens of fresher ($S \sim 34.66 \text{ psu}$)

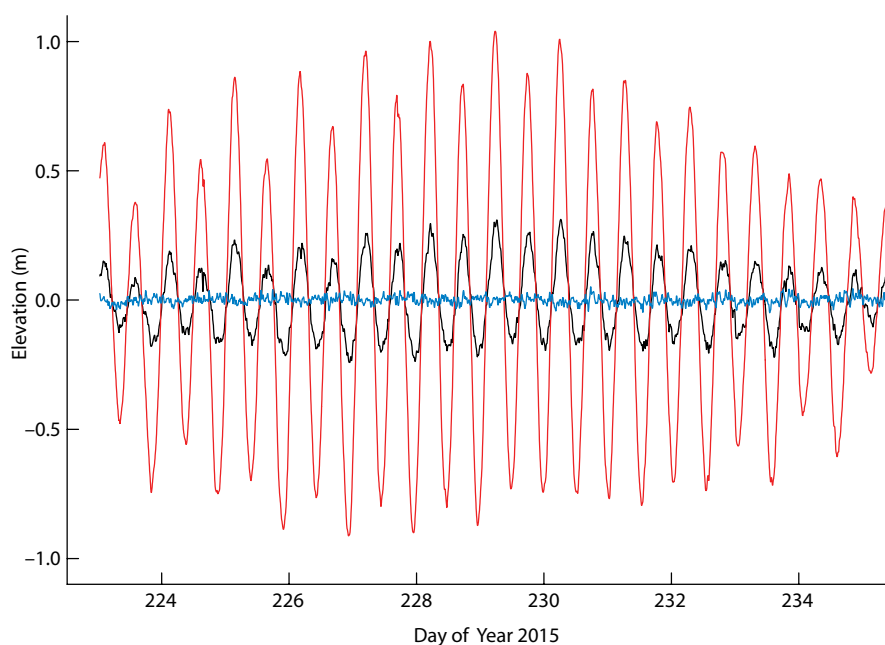


FIGURE 4. Time series of vertical displacement of three GPS antennas placed on Petermann Gletscher for 13 days in August of 2015. Colors indicate position of stations: (red) 26 km seaward of the grounding zone (GZ+26), (black) in the grounding zone (GZ-00), and (blue) 20 km landward of the grounding zone (GZ-20). Note the strong semidiurnal tidal oscillations diminishing toward the grounding zone.

and colder ($T \sim -0.1^\circ\text{C}$) water at a location where the ice island had been a few days before (Figure 5). We speculate that local melting and vertical mixing below the rapidly moving ice island caused this T-S anomaly whose sloping density contours (isopycnals) suggest a 10 km wide clockwise-rotating eddy.

Density contours slope strongly from 300 m to 400 m depth in Nares Strait and from 500 m to 600 m depth in Petermann Fjord within about 10 km of the sill. Such sloping isopycnals imply ocean currents and ocean dynamics that we have not yet fully explored. For example, the

deepening isopycnals toward the sill imply a clockwise circulation, if baroclinic pressure gradients are balanced by the Coriolis force. H. Johnson et al. (2011) and Shroyer et al. (in press) present observations and model results that expand on dynamical implications of such interactions between Petermann Fjord and adjacent Nares Strait.

OCEAN OBSERVATIONS BELOW PETERMANN GLETSCHER

In August 2015, the icebreaker *Oden* visited Petermann Fjord as part of an interdisciplinary study to reconstruct its

Holocene history, building on a single sediment core from the adjacent Hall Basin in Nares Strait (Jennings et al., 2011). Cruise participants mapped bottom topography, collected sediment cores, and measured water properties in Nares Strait, Petermann Fjord, and under the ice shelf of Petermann Gletscher. Access to the ocean and the sediments beneath the ice shelf was provided by 0.3 m wide access holes created by hot water drilling (Makinson and Anker, 2014) at three sites (see Figure 2 for locations). At two sites, we drilled through ~100 m of ice within the central channel 16 km and 26 km seaward of the grounding zone. A third station was placed within 3 km of the grounding zone, again within the central channel, where the ice shelf was 365 m thick.

We present preliminary results from our central site. We deployed an Ocean Weather Station that connects five internally powered SBE 37-sm ocean sensors with conducting cables through the ice shelf to Campbell CR1000 data loggers at the surface. The data loggers distribute power from two 12 V rechargeable batteries to sensors of an automatic weather station, a single frequency GPS, and an Iridium satellite modem. The data loggers receive and process ocean data (temperature, conductivity, and pressure) as well as atmospheric data (temperature, humidity, pressure, wind speed, and wind direction). In turn, the data loggers connect to an Iridium modem designed to allow real-time access both to data and to processing software. The station was successfully installed on August 20, 2015, and provided a gap-free data set via the Iridium link until February 11, 2016, when we last connected to the station until a maintenance visit on August 27, 2016, when a full record was retrieved and connectivity restored with the so-called Circuit Switched Data.

The ocean sensors were calibrated against a Sea-Bird 911+ sensor system in Nares Strait two weeks prior to their deployment below the ice shelf. The sensors were placed on a Kevlar mooring

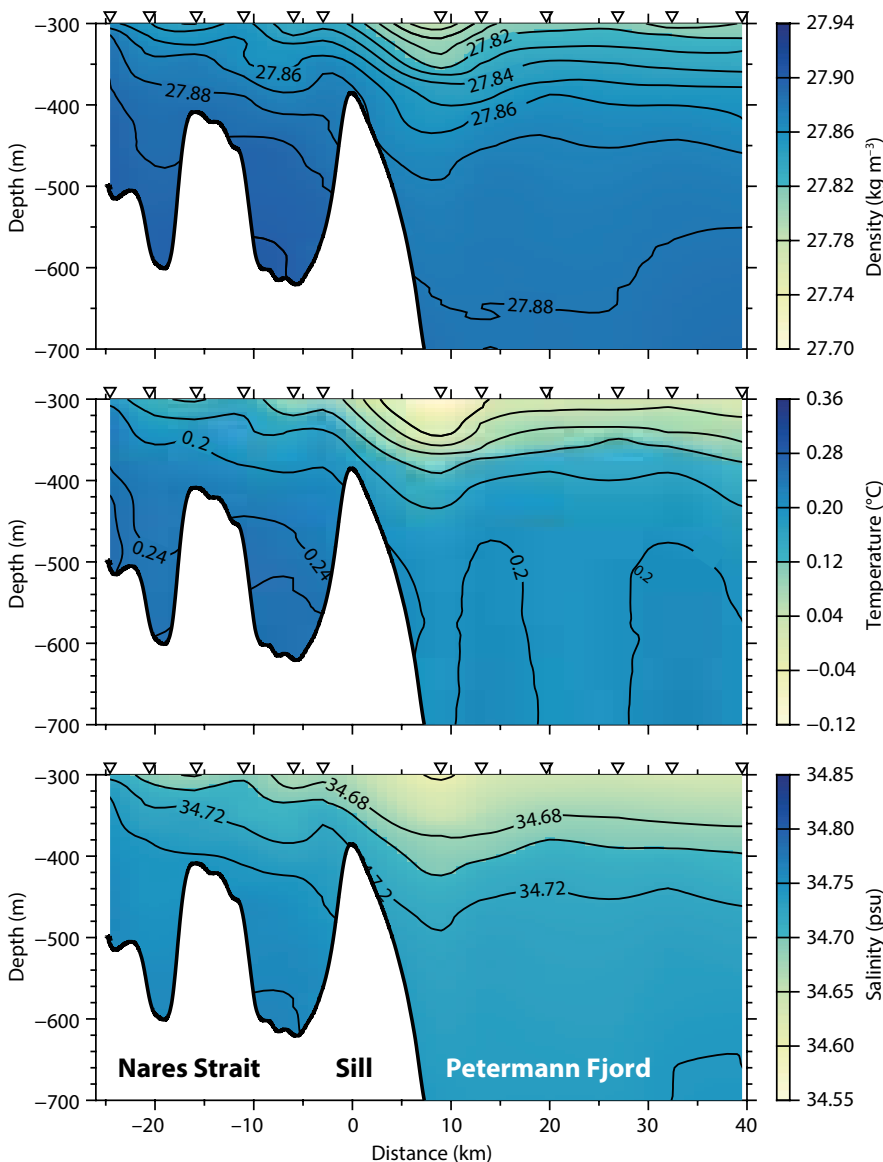


FIGURE 5. Section for depths below 300 m from Nares Strait to the terminus of Petermann Gletscher showing the density anomaly in kg m^{-3} (top panel), potential temperature in $^\circ\text{C}$ (middle panel), and salinity in psu (bottom panel) as observed on August 10–11, 2012.

line at nominal depths of about 95 m, 115 m, 300 m, 450 m, and 810 m below sea level. At the time of deployment, the bottom of the ice shelf and the seafloor at this site were about 90 m and 840 m below sea level. The ice shelf moves vertically about 2 m with the dominantly semidiurnal tides (Figure 4) but, because the moorings are fixed to the ice shelf, they move vertically as well, maintaining their distance below the sea surface. Prior to deploying the mooring, a CTD profile was obtained from the ice shelf base to the seabed.

We compared the calibrated mooring data from the 170-day record with the CTD profile at the mooring location and a profile from Nares Strait (Figure 6). The moored observations occupy the same region in T-S space as that of the CTD. The densest water at the mooring is the most saline, which in Petermann Fjord is also the warmest water. Temperatures at the deepest sensors sometimes exceed +0.3°C.

The Nares Strait profile shows a distinct temperature maximum at a salinity of 34.80 psu, which is significantly saltier than the 34.76 psu observed there in 2012 and earlier. At our ice shelf mooring site, the salinity at 810 m depth is always below 34.78 psu, measured by CTD profiling (purple line) and by the moored sensors (symbols). As an aside, the Nares Strait cast is the first observation in Nares Strait that shows the core of the Atlantic Water as a distinct temperature maximum. Such waters have never before been observed crossing the northern 290 m deep sill in the Lincoln Sea to enter Nares Strait (see Figure 1 for locations). We speculate that this core of Atlantic Water will be present both inside Petermann Fjord and under its ice shelf within a year or two.

Data that fall onto a straight line in T-S space indicate mixing of two distinct water masses. The two CTD profiles in Figure 6 represent two mixing lines that form a triangle whose corners we define as three distinct water masses. These are Atlantic Water (AW), Glacier Melt Water

(GMW), and Polar Water (PW). The Nares Strait CTD profile slopes gently as it connects AW to PW, whereas the ice shelf CTD profile slopes more steeply as it connects the same AW to GMW. The salinity of the AW end member in Petermann Fjord is $S_{AW} = 34.76$ psu and the potential temperature is $\theta_{AW} = +0.3^\circ\text{C}$. The effective temperature of GMW depends on the latent heat that is required for the transition of solid glacier ice to liquid freshwater. If we assume that this heat is extracted from the ambient ocean with temperature θ_{AW} and salinity S_{AW} , then the melting of ice reduces the ambient θ_{AW} to the in situ T_{gade} ,

$$T_{gade}(S) = \theta_{AW} + L_f/c_p (1 - S_{AW}/S),$$

where S is the observed in situ ocean salinity, $L_f = 334 \text{ kJ kg}^{-1}$ is the latent heat of fusion, and $c_p = 3.97 \text{ kJ kg}^{-1} \text{ K}^{-1}$ is the specific heat of water with salinity S_{AW} (Wählin et al., 2010). Observed temperatures and salinities result from the mixing of ambient AW with GMW to create a mixing line (Gade, 1979); see Figure 6. It closely corresponds to the

CTD profile from under the ice shelf for $\sigma_\theta < 27.88 \text{ kg m}^{-3}$ (roughly 400 m depth) and demonstrates that our observations in the upper ocean under the ice shelf represent a mixture of AW with GMW. Consistent with this, mooring data from 300 m fall along this Gade line. In contrast, mooring data at 450 m depth and 810 m fall on another mixing line that more closely aligns with waters observed in Nares Strait. These deeper waters contain no glacier meltwaters at this location. We thus speculate that the deep AW flowing toward the grounding line does not interact with the ice shelf; however, these waters then melt the glacier near the grounding zone at 450 m to 600 m depth to produce a mixture of AW and GMW that then, we speculate, rises vertically on account of its buoyancy, pools in local channels within the base of the ice shelf, and returns up to the ice shelf base toward our mooring site. The scatter of the moored observations results from temporal variability in glacier-ocean interactions that we discuss below.

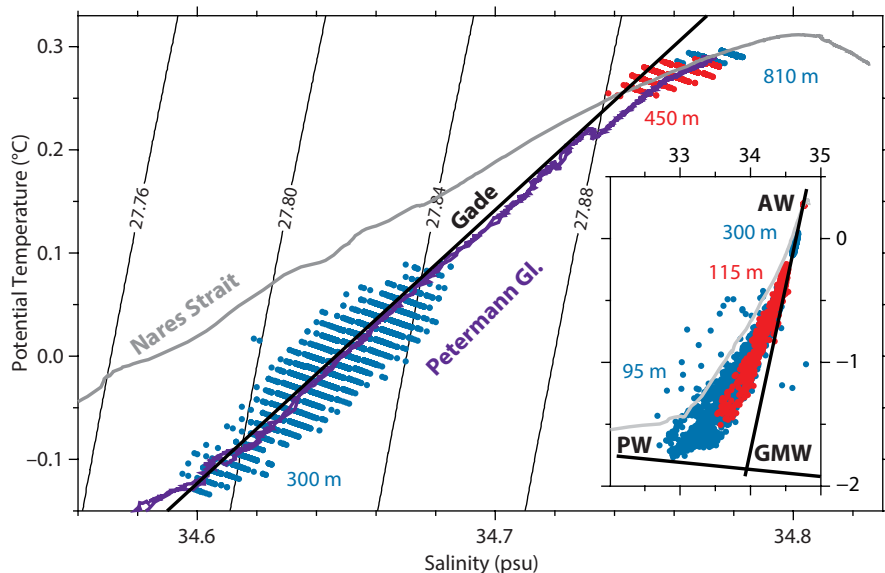


FIGURE 6. Temperature and salinity from moorings (symbols representing nominal sensor depths at 300 m, 450 m, and 810 m below sea level) and two 2015 CTD casts. The purple line labeled Petermann Gl. indicates water properties under the ice shelf on August 20, 2015, at the location and time when the ocean moorings were deployed. The faint gray line labeled Nares Strait shows properties from Nares Strait (August 21, 2015), and the black line shows the theoretical Gade line. Contours are density anomalies in kg m^{-3} . Insert includes data from 95 m and 115 m on expanded scales along with Gade and freezing lines and relative locations of Atlantic Water (AW), Polar Water (PW), and Glacier Melt Water (GMW) in θ - S space. The GMW end member has a salinity of zero on the Gade mixing line.

Time series of ocean salinity (S) and potential temperature (θ) at fixed depths between 95 m and 450 m below sea level from August 20, 2015, to February 11, 2016, (Figure 7) show depth-dependent variability on a broad range of time scales. The 810 m record is not shown, as it is indistinguishable from the 450 m record at this scale. The hourly data were low-pass filtered to remove tidal and daily variability. Within about 20 m of the ice shelf base, at the sensors located 95 m and 115 m below sea level, we find large oscillations in θ and S that swing between a fresher and colder state ($S \sim 33.4$ psu, $\theta \sim -1.4^\circ\text{C}$) and a saltier and warmer ($S \sim 34.4$, $\theta \sim -0.3^\circ\text{C}$) state. Pulses of the fresh and cold waters arrive predictably twice every month for the first four months of the record, when signals exceed 0.8°C and 0.5 psu. We speculate that our sensors are resolving large and periodic changes in mixed layer thickness and θ - S properties. Based on comparisons from measurements under other ice shelves (e.g., Nicholls et al., 2009), we

speculate that these pulses are caused by spring/neap tidal modulation of basal meltwater production and/or advection below the ice shelf.

The bimonthly variations do not extend down to sensors at 300 m and 450 m below sea level. At 300 m we find smaller, albeit still detectable, signals with temporal fluctuations of about 0.1°C (Figures 6 and 7) over a broader range of periodicities (not shown). Nevertheless, both θ and S increase with depth, and our deep sensors record the same AW characteristics that we find in Petermann Fjord seaward of the terminus of the ice shelf. Our 2015/16 mooring data reveal a mean value for θ of $0.00 \pm 0.037^\circ\text{C}$ at 300 m and $+0.28 \pm 0.006^\circ\text{C}$ at 450 m depth, where the uncertainty is one standard deviation from the mean. Mean values of S are 34.65 ± 0.014 psu (300 m), 34.76 ± 0.007 psu (450 m), and 34.77 ± 0.006 psu (810 m). This justifies the ambient AW salinity of $S_{\text{AW}} = 34.76$ psu used in the calculation of the Gade line here and in H. Johnson et al. (2011).

DISCUSSION

Decay, retreat, and eventual collapse represent three increasingly dramatic phases of ice shelf loss around Greenland (Motyka et al., 2011) and Antarctica (Glasser et al., 2009). Dramatic collapse of Jakobshavn Isbrae in Southwest Greenland (Motyka et al., 2011) and Zachariae Isstrom in Northwest Greenland (Mouginot et al., 2015) have been attributed to warm ocean waters that reach the glaciers and increase basal melt rates. The ice shelves of both Petermann and Nioghalvfjerdingsfjorden Glaciers are presently thinning and their termini are retreating. We propose that they are poised for further retreat and potential collapse as air and ocean temperatures around northern Greenland continue to increase. Previous ice shelf collapses further south in Greenland, and in West Antarctica, have led to rapid retreat of grounding lines and accelerated loss of grounded ice. We would like to be able to predict the fate of remaining Greenland ice shelf systems to help reduce uncertainty in future contributions of grounded ice loss to global sea level change. Our studies of the Petermann system provide insight into the behavior and sensitivity of an important outlet glacier for the Greenland Ice Sheet. These results also point to the benefits of continuous sensing of this and similar glacier systems at tidal to inter-annual time scales.

Historically, the discharge of ice across the grounding zone of Petermann Gletscher has been balanced mostly by ocean melting of its floating ice shelf, while calving flux and surface ablation of the ice shelf were smaller (Rignot and Steffen, 2008). The sum of these terms amounted to approximate mass balance. However, geostrophic current estimates (H. Johnson et al., 2011) indicate that heat flux into the fjord across its sill is a factor of three to six times higher than needed to maintain the ice shelf in steady state, suggesting that small changes in the heat content of water flowing into the fjord and in the efficiency of ice-ocean interactions could substantially alter ice

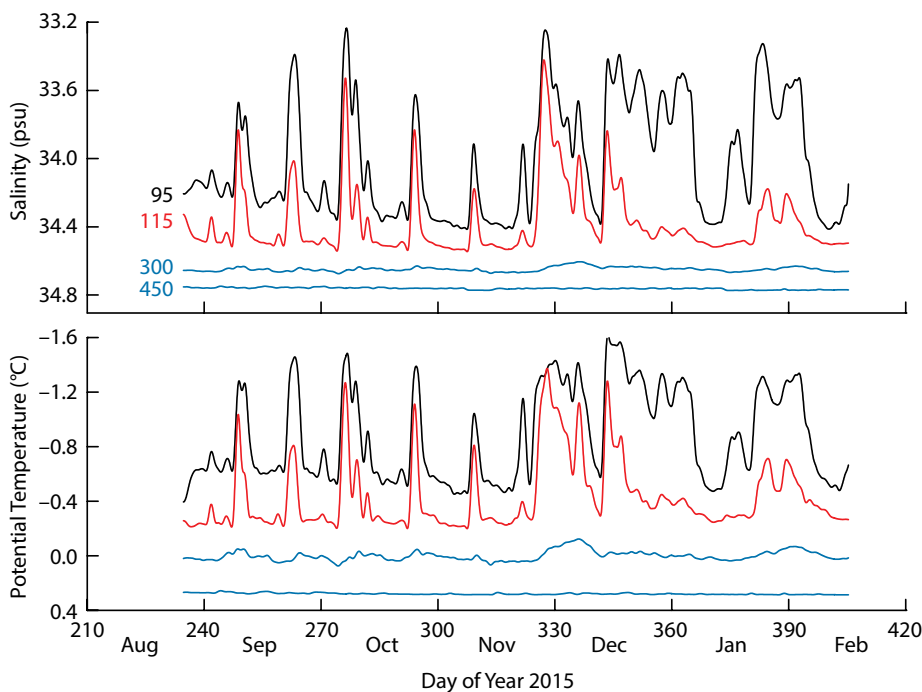


FIGURE 7. Time series of salinity (top) and potential temperature (bottom) from four ocean sensors deployed under the ice shelf of Petermann Gletscher from August 20, 2015, through February 11, 2016. Temperature and salinity scales are inverted in order to emphasize the vertical arrangements of sensors deployed at 95 m (black), 115 m (red), and 300 m and 450 m (blue) below sea level. Note the large fortnightly oscillations under the ice shelf at 95 m and 115 m depth in the first half of the record.

shelf loss by melting. Modeling ice-ocean interactions with realistic bottom topography revealed sensitivity of Petermann Gletscher ice shelf basal melting to changes in Nares Strait ocean dynamics that are caused by the seasonal cycle of sea-ice mobility, from winter fast ice to summer mobile ice cover (Shroyer et al., in press). Interannual and longer-term changes in Nares Strait sea ice, perhaps associated with the long-term thinning trend of Arctic Ocean sea ice, could therefore alter the glacier mass balance.

At the same time, the long-term trend of atmospheric warming over Greenland (Hanna et al., 2008) is expected to increase mass loss by seasonal surface melting on both the grounded ice and the ice shelf. The subglacial discharge of freshwater across the grounding line is believed to accelerate ice shelf basal melting near the grounding line (e.g., Motyka et al., 2003, 2011; Straneo et al., 2013); therefore, we expect higher ice-shelf basal melt rates in warmer summers. Iceberg production is also expected to increase as more rapid thinning from basal melting, combined with rift growth as liquid freshwater drains into surface crevasses to cause “hydrofracture” of the ice shelf (Scambos et al., 2003), increases potential for calving. These three processes are intricately related: a retreating ice front changes ocean circulation within the fjord (H. Johnson et al., 2011), a thinning ice shelf increases the likelihood of iceberg calving as vertical crevasses grow (Bassis and Ma, 2015), and the increased flux of surface-produced liquid freshwater across the grounding line accelerates basal melting near the grounding line to alter fjord stratification and, potentially, reduce the ocean heat available to the base of the thinner outer portions of the ice shelf.

We speculate that the exceptionally large calving losses at Petermann Gletscher in 2010 and 2012 may indicate a transition to a new, but possibly temporary, quasi-equilibrium state with an ice shelf length of about 50 km instead of 70–80 km. Some evidence for a

new equilibrium is provided by Figure 8, which shows a large fracture that is likely to become the future terminus. Both the 2010 and 2012 ice islands resulted from similar fractures that formed ice islands when the fracture reached the central channel. We expect that this fracture will form another ice island, perhaps 120–150 km² in area and ~25–30 km³ in volume, within the next few years, well before the ice front advances to its old (pre-2010) location.

In this new equilibrium, the balance between calving and basal melting would be different from the earlier estimates. Assuming that the typical terminus ice thickness is ~200 m, which is consistent with the 2012 and the expected next calving event, the “steady state” calving flux

will be ~3 km³ yr⁻¹. This value is several times higher than the much earlier estimate of 0.46 km³ yr⁻¹ by Higgins (1990), who used a mean thickness of 40 m for calving ice. However, this new calving flux remains a relatively small fraction of the total ice volume crossing the grounding line, so that most mass loss would still occur through basal melting. Changes in basal melt rate driven by variability in AW inflow or by subglacial freshwater discharge across the grounding line (or both) are, therefore, likely to determine whether the ice shelf stabilizes at its new length or if continued retreat will occur.

The improved frequency and accuracy of satellite and airborne observations of ice sheet and ice shelf velocity, extent, and thickness have helped develop our




FIGURE 8. Northeastern section of Petermann Gletscher’s floating ice shelf as seen by Landsat at 15 m resolution on August 10, 2015. Hall Land is visible in the top right corner while the terminus and fjord are visible in the top left corner (see Figure 2 for location). The central channel appears on the left, and a large lateral fracture emanates from the marginal shear zone. Smaller such fractures appear spaced about 1.2 km apart. Both 2010 and 2012 calving events were triggered by such fractures when they reached the central channel.

appreciation for the time scales and major drivers of change in Greenland Ice Sheet mass balance. However, as shown here, many critical processes are not resolved by remote sensing or by occasional, short-term ship-based surveys of the ocean regions near the ice sheet's marine margins. Summer-only measurements, constrained by ship access to fjords, fail to identify processes that dominate in winter. Our new hydrographic measurements under the ice shelf implicate tidal processes in basal meltwater production and/or transport and suggest a transition in the character of meltwater production and/or advection through the winter. Realistic regional high-resolution modeling suggests that eddies and instabilities of the southward flow through Nares Strait, with time scales of order 10 days, can substantially increase ocean heat transport into Petermann Fjord (Shroyer et al., in press). The time scale relates to dynamical forcing of both surface stress and remote wind fields that cause Ekman flux across and pressure gradients along Nares Strait (Münchow, 2016). This process is tied to sea-ice state in Nares Strait, bringing another layer of complexity to modeling Petermann Gletscher on inter-annual and longer time scales. Unless models represent this variability correctly, they are unlikely to provide reliable projections for ice sheet response to future climate states.

CONCLUSION

Petermann Gletscher today terminates as a ~50 km long floating ice shelf after losing about one-third of its area in two large calving events in 2010 and 2012. This calving resulted in Manhattan-sized ice islands that then drifted into the Labrador Sea via Nares Strait and Baffin Bay. The 2013/14 and 2015/16 flow speeds of the ice shelf are $12 \pm 5\%$ larger than they were during the prior decade, and the ice shelf was observed to thin for at least several years prior to the 2010 calving event. Assuming that the current configuration of the ice shelf (shorter and with a thicker terminus) represents

a new equilibrium, the calving flux has increased about sixfold relative to twentieth century values. These observations suggest that the ice shelf of Petermann Gletscher is not currently in steady state. Ocean observations from both the fjord and the glacier cavity indicate potential for large changes in ice-ocean thermodynamic interactions as Atlantic-sourced ocean waters below Petermann Gletscher ice shelf become warmer and saltier. A subglacial ocean observatory reporting ocean properties hourly reveals large fortnightly pulses of cold and fresh water within 25 m of the ocean-glacier interface. Amplitudes of these pulses are larger than 1 psu in salinity and 1°C in temperature. We posit that episodic discharge of glacial meltwater modulated by the spring-neap tidal cycle thickens the boundary layer under the ice shelf at the location of our measurements. Sustained time series observations adjacent to and under Greenland's glaciers during both winter and summer are much needed to quantify and dynamically understand glacier-ocean interactions. 

REFERENCES

- Ahlstrom, A.P., S.B. Andersen, M.L. Andersen, H. Machguth, F.M. Nick, I. Joughin, C.H. Reijmer, R.S.W. van de Wal, J.P. Merryman Boncori, J.E. Box, and others. 2013. Seasonal velocities of eight major marine-terminating outlet glaciers of the Greenland ice sheet from continuous in situ GPS instruments. *Earth Systems Science Data* 5:277–287, <https://doi.org/10.5194/essd-5-277-2013>.
- Ahnert, F. 1963. The terminal disintegration of Steensby Gletscher, North Greenland. *Journal of Glaciology* 4(35):537–545.
- Antoniades, D., P. Francus, G. St-Onge, and W.F. Vincent. 2011. Holocene dynamics of the Arctic's largest ice shelf. *Proceedings of the National Academy of Sciences of the United States of America* 108(47):18,899–18,904, <https://doi.org/10.1073/pnas.1106378108>.
- Bamber, J.L., M.J. Siegert, J.A. Griggs, S.J. Marshall, and G. Spada. 2013. Paleofluvial mega-canyon beneath the central Greenland ice sheet. *Science* 341:997–999, <https://doi.org/10.1126/science.1239794>.
- Bassis, J.N., and Y. Ma. 2015. Evolution of basal crevasses links ice shelf stability to ocean forcing. *Earth and Planetary Science Letters* 409(1):203–211, <https://doi.org/10.1016/j.epsl.2014.11.003>.
- Boas, F. 1885. Baffin-Land, geographische Ergebnisse einer in den Jahren 1883 und 1884 ausgeführten Forschungsreise. *Petermann's Mitteilungen Ergänzungsheft* 80:1–100.
- Coachman, L.K., and C.A. Barnes. 1963. The movement of Atlantic Water in the Arctic Ocean. *Arctic* 16:9–16.
- Crawford, A.J., P. Wadhams, T.J.W. Wagner, A. Stern, E.P. Abrahamson, I. Church, R. Bates, and K.W. Nicholls. 2016. Journey of an Arctic ice island. *Oceanography* 29(2):254–263, <https://doi.org/10.5670/oceanog.2016.30>.
- de Steur, L., M. Steele, E. Hansen, J. Morison, I. Polyakov, S.M. Olsen, H. Melling, F.A. McLaughlin, R. Kwok, W.M. Smethie Jr., and P. Schlosser. 2013. Hydrographic changes in the Lincoln Sea in the Arctic Ocean with focus on an upper ocean freshwater anomaly between 2007 and 2010. *Journal of Geophysical Research* 118:4,699–4,715, <https://doi.org/10.1002/jgrc.20341>.
- Freuchen, P. 1935. *Arctic Adventures: My Life in the Frozen North*. Farrar & Rinehard, New York, 467 pp.
- Fricke, H.A., and L. Padman. 2006. Ice shelf grounding zone structure from ICESat laser altimeter. *Geophysical Research Letters* 33, L15502, <https://doi.org/10.1029/2006GL026907>.
- Glasser, N.F., B. Kulesa, A. Luckman, D. Jansen, E.C. King, P.R. Sammonds, T.A. Scambos, and K.C. Jezek. 2009. Surface structure and stability of the Larsen C ice shelf, Antarctic Peninsula. *Journal of Glaciology* 55:400–410.
- Gade, H.G. 1979. Melting of ice in sea water: A primitive model with application to the Antarctic ice shelf and icebergs. *Journal of Physical Oceanography* 9:189–198.
- Gladish, C.V., D.M. Holland, P.R. Holland, and S.F. Price. 2012. Ice-shelf basal channels in a coupled ice/ocean model. *Journal of Glaciology* 58 (212):1,227–1,244, <https://doi.org/10.3189/2012JoG12J003>.
- Greely, A.W. 1888. *Report on the Proceedings of the United States Expedition to Lady Franklin Bay, Grinnell Land*. Government Printing Office, Washington, DC.
- Hanna, E., P. Huybrechts, K. Steffen, J. Cappelen, R. Huff, C. Shuman, T. Irvine-Fynn, S. Weiss, and M. Griffiths. 2008. Increased runoff from the Greenland ice sheet: A response to global warming. *Journal of Climate* 21:331–341, <https://doi.org/10.1175/2007JCLI1964.1>.
- Hanna, E., F.J. Navarro, F. Pattyn, C.M. Domingues, X. Fettweis, E.R. Ivins, R.J. Nicholls, C. Ritz, B. Smith, S. Tulaczyk, and others. 2013. Ice-sheet mass balance and climate change. *Nature* 498:51–59, <https://doi.org/10.1038/nature12238>.
- Harris, R.A. 1911. *Arctic Tides*. Government Printing Office, Washington, DC.
- Hattersley-Smith, G., L.S. Koenig, K.R. Greenaway, and M. Dunbar. 1952. Arctic ice islands. *Arctic* 5:67–103, <https://doi.org/10.14430/arctic3901>.
- Higgins, A.K. 1990. North Greenland glacier velocities and calf ice production. *Polarforschung* 60(1):1–23.
- Jeffries, M. 1992. Arctic ice shelves and ice islands: Origin, growth, and disintegration, physical characteristics, structural-stratigraphic variability, and dynamics. *Reviews of Geophysics* 30(3):245–267, <https://doi.org/10.1029/92RG00956>.
- Jennings, A.E., C. Sheldon, T.M. Cronin, P. Francus, J. Stoner, and J. Andrews. 2011. The Holocene history of Nares Strait. *Oceanography* 24(3):26–41, <https://doi.org/10.5670/oceanog.2011.52>.
- Johnson, H.L., A. Münchow, K.K. Falkner, and H. Melling. 2011. Ocean circulation and properties in Petermann Fjord, Greenland. *Journal Geophysical Research* 116, C01003, <https://doi.org/10.1029/2010JC006519>.
- Johnson, J.P. 1990. The establishment of Alert, NWT, Canada. *Arctic* 43 (1):21–34.
- Joughin, I., B.E. Smith, I.M. Howat, T. Scambos, and T. Moon. 2010. Greenland flow variability from ice-sheet wide velocity mapping. *Journal of Glaciology* 56(197):415–430, <https://doi.org/10.3189/002214310792447734>.

- King, B. 2004. Rigorous GPS data-processing strategies for glaciological applications. *Journal of Glaciology* 50(171):601–607, <https://doi.org/10.3189/172756504781829747>.
- Koch, L. 1928. Contributions to the glaciology of North Greenland. *Meddelelser om Gronland* 65:181–464.
- Makinson, K., and P.G.D. Anker. 2014. The BAS ice-shelf hot-water drill: Design, methods, and tools. *Annals of Glaciology* 55(68):44–55, <https://doi.org/10.3189/2014AoG68A030>.
- Millgate, T., P.R. Holland, A. Jenkins, and H.L. Johnson. 2013. The effect of basal channels on oceanic ice-shelf melting. *Journal of Geophysical Research* 118 (12):6,951–6,964, <https://doi.org/10.1002/2013JC009402>.
- Mouginot, J., E. Rignot, B. Scheuchl, I. Fenti, A. Khanzendar, M. Morlighem, A. Buzzi, and J. Paden. 2015. Fast retreat of Zachariae Isstrom, Northeast Greenland. *Science* 350:1,357–1,361, <https://doi.org/10.1126/science.aac7111>.
- Motyka, R.J., L. Hunter, K.A. Echelmeyer, and C. Connor. 2003. Submarine melting at the terminus of a temperate tidewater glacier, LeConte Glacier, Alaska, USA. *Annals of Glaciology* 36(1):57–65, <https://doi.org/10.3189/172756403781816374>.
- Motyka, R.J., M. Truffer, M. Fahnestock, J. Mortensen, S. Rysgaard, and I. Howat. 2011. Submarine melting of the 1985 Jakobshavn Isbrae floating tongue and the triggering of the current retreat. *Journal of Geophysical Research* 116, F01007, <https://doi.org/10.1029/2009JF001632>.
- Münchow, A. 2016. Volume and freshwater flux observations from Nares Strait to the west of Greenland 2003 to 2009. *Journal of Physical Oceanography* 46(1):141–157, <https://doi.org/10.1175/JPO-D-15-00931>.
- Münchow, A., K.K. Falkner, and H. Melling. 2015. Baffin Island and West Greenland current systems in northern Baffin Bay. *Progress in Oceanography* 132:305–317, <https://doi.org/10.1016/j.pocean.2014.04.001>.
- Münchow, A., K.K. Falkner, H. Melling, B. Rabe, and H.L. Johnson. 2011. Ocean warming of Nares Strait bottom waters off Northwest Greenland 2003–2009. *Oceanography* 24(3):114–123, <https://doi.org/10.5670/oceanog.2011.62>.
- Münchow, A., L. Padman, and H.A. Fricker. 2014. Interannual changes of the floating ice shelf of Petermann Gletscher, North Greenland, from 2000 to 2012. *Journal of Glaciology* 60(221):489–499, <https://doi.org/10.3189/2014JoG13J135>.
- Nares, G. 1876. *The Official Report of the Recent Arctic Expedition*. John Murray, London, UK.
- Nicholls, K.W., S. Osterhus, K. Makinson, and T. Gammelsrod. 2009. Ice-ocean processes over the continental shelf of the southern Weddell Sea, Antarctica: A Review. *Reviews of Geophysics* 47, RG3003, <https://doi.org/10.1029/2007RG000250>.
- Nick, F.M., A. Luckman, A. Vieli, C.J. Van Der Veen, D. Van As, R.S.W. Van De Wal, F. Pattyn, A.L. Hubbard, and D. Floricioiu. 2012. The response of Petermann Glacier, Greenland, to large calving events, and its future stability in the context of atmospheric and oceanic warming. *Journal of Glaciology* 58 (208):229–239, <https://doi.org/10.3189/2012JoG11J242>.
- Polyakov, I.V., L.A. Timokhov, V.A. Alexeev, S. Bacon, I.A. Dmitrenko, L. Fortier, I.E. Frolov, J.-C. Gascard, E. Hansen, V.V. Ivanov, and others. 2010. Arctic Ocean warming contributes to reduced polar ice cap. *Journal of Physical Oceanography* 40:2,743–2,756, <https://doi.org/10.1175/2010JPO4339.1>.
- Rasmussen, K. 1921. *Greenland by the Polar Sea: The Story of the Thule Expedition from Melville Bay to Cape Morris Jessup*. Translated from the Danish by Asta and Rowland Kenney, Frederick A. Stokes, New York, NY, 327 pp.
- Rignot, E. 1996. Tidal motion, ice velocity and melt rate of Petermann Gletscher, Greenland, measured from radar interferometry. *Journal of Glaciology* 42(142):476–485.
- Rignot, E., S. Gogineni, I. Joughin, and W. Krabill. 2001. Contribution to the glaciology of northern Greenland from satellite radar interferometry. *Journal of Geophysical Research* 106(D24):34,007–34,019, <https://doi.org/10.1029/2001JD900071>.
- Rignot, E., and K. Steffen. 2008. Channelized bottom melting and stability of floating ice shelves. *Geophysical Research Letters* 35, L02503, <https://doi.org/10.1029/2007GL031765>.
- Scambos, T.A., C. Hulbe, and M.A. Fahnestock. 2003. Climate-induced ice shelf disintegration in the Antarctic Peninsula. Pp.79–92 in *Antarctic Peninsula Climate Variability: A Historical and Paleoenvironmental Perspective*. Antarctic Research Series, vol. 79, E. Domack, A. Levente, A. Burnet, R. Bindshadler, P. Convey, and M. Kirby, eds, American Geophysical Union, Washington, DC, <https://doi.org/10.1029/AR079p0079>.
- Shroyer, E.L., L. Padman, R.M. Samelson, A. Münchow, and L. Stearns. In press. Control of Petermann Gletscher ice-shelf melt by sea-ice and ocean circulation in Nares Strait. *Journal of Glaciology*.
- Straneo, F., and P. Heimbach. 2013. North Atlantic warming and the retreat of Greenland's outlet glaciers. *Nature* 504:36–43, <https://doi.org/10.1038/nature12854>.
- Straneo, F., P. Heimbach, O. Sergienko, G. Hamilton, G. Catania, S. Griffies, R. Hallberg, A. Jenkins, I. Joughin, R. Motyka, and others. 2013. Challenges to understanding the dynamic response of Greenland's marine terminating glaciers to oceanic and atmospheric forcing. *Bulletin of the American Meteorological Society* 94:1,131–1,144, <https://doi.org/10.1175/BAMS-D-12-00100.1>.
- Wåhlin, A.K., X. Yuan, G. Björk, and C. Nohr. 2011. Inflow of warm Circumpolar Deep Water in the central Amundsen Sea. *Journal of Physical Oceanography* 40:1,427–1,434, <https://doi.org/10.1175/2010JPO4431.1>.

AUTHORS

Andreas Münchow (muenchow@udel.edu) is Associate Professor, University of Delaware, Newark, DE, USA. **Laurie Padman** is Senior Scientist, Earth & Space Research, Corvallis, OR, USA. **Peter Washam** is Graduate Student, University of Delaware, Newark, DE, USA. **Keith W. Nicholls** is Oceanographer, British Antarctic Survey, Cambridge, UK.

ARTICLE CITATION

Münchow, A., L. Padman, P. Washam, and K.W. Nicholls. 2016. The ice shelf of Petermann Gletscher, North Greenland, and its connection to the Arctic and Atlantic Oceans. *Oceanography* 29(4):84–95, <https://doi.org/10.5670/oceanog.2016.101>.

ACKNOWLEDGMENTS

Both the National Science Foundation (NSF) and National Aeronautics and Space Administration (NASA) supported this work over many years. We are grateful to crew and staff aboard the Canadian Coast Guard Ship Henry Larsen in 2012 and the Swedish icebreaker Oden in 2015. Humfrey Melling of the Institute of Ocean Sciences and Alan Mix of Oregon State University generously shared time and resources at sea in 2012 and 2015. The 2015 bottom bathymetry data were kindly provided to us at sea in preliminary form by Martin Jakobsson of the University of Stockholm and Larry Mayer of the University of New Hampshire. Anna Wåhlin of Gothenburg University, Sweden, provided the CTD system used aboard the 2015 Oden expedition that was jointly funded by NSF and the Swedish Polar Research Secretariat. Paul Anker and Mike Brian of the British Antarctic Survey provided critical support for hot water drilling and glacier traveling. The Ocean Weather Station was designed and built by David Huntley at the University of Delaware and funded by NASA grant NNX15AL77G. AM was supported by a subcontract from Jet Propulsion Laboratory in 2015 as part of the Oceans Melting Greenland mission and NSF grants 102843 and 1604076 in 2012 and